




Experimental and Theoretical Study of the Measured Wavelength of Laser Light Using Mach–Zehnder interferometer

H. Naser* , H. M. Shanshool, S. F. Hassan and A. B. Dheyab

Directorate of Material Research, Ministry of Science and Technology, Baghdad, Iraq

Received: 14 July 2018 / Accepted: 22 March 2019

© Metrology Society of India 2019

Abstract: In this research, the experimental and theoretical studies to measure the wavelength of laser light by Mach–Zehnder interferometer were conducted. Then, the results were compared with Zemax software. The fringes have been obtained both as shining and dark. The wavelength of laser light and the diameter of fringes were calculated by the optical system. The calculation relies on the measure of the airy disk diameter, whose approximation is directly proportional to the wavelength of the laser source; and to the space between the aperture and the image plane. However, the calculation is reciprocally proportional to the diameter of the aperture. Then, the results were compared with Zemax software, where the ratio of error is very small.

Keywords: Mach–Zehnder; Diode laser; Interference fringes; Ray-tracing software

1. Introduction

In physics, the MZI is an instrument used to decide the relative stage move varieties between two collimated beams obtained by splitting light from a solitary source. The interferometer has been utilized, in addition to admeasurement phase shifts between the two beams caused by a specimen or an adjustable length of one of the ways. The mechanical assembly is named after the physicists Ludwig Mach (the child of Ernst Mach) and Ludwig Zehnder. Zehnder's proposition in an 1891 article was refined by Mach in an 1892 article [1–4]. It was decided to produce fringes in white light at that point, since white light has a restricted intelligence length. On the request of micrometers, extreme care should be taken into account, while for the remaining optical ways for all wavelengths or no fringes will be noticeable. Also, the accurate orientation of the ray splitters was noticed. The ray splitters' reflecting surfaces were also located. Thus, the test and reference beams go through air. In this introduction, the test and reference ray experience two front surface reflections, bringing about a similar number of stage reversals. The outcome is that light voyaging an equivalent optical way length in the test and reference fabricated a laser light edge

of productive impedance. It was found that when an interferometer is lit up by a laser source, it is framed by a discrete arrangement of focuses or lines [5].

All interferometry techniques depend on the impedance design shaped by the superposition of light waves which start from the same source; cross special ways. So the fringe design shaped by these shafts shows the local phase shifts appear from the distinction in the optical ways crossed by the meddling rays.

The most widely recognized interferometers are Fizeau interferometer, Michelson interferometer, Fabry–Perot interferometer, Jamin interferometer, Ramsey–Borde interferometer and Mach–Zehnder ones [6].

The major base of wavelength interferometry is presented and its benefits and bad marks are brought up [7]. Zemax software could be a ray-tracing software system that not only will exclude style and analyze imaging, but also as illumination systems. Moreover, Zemax used the design of lenses, gratings, lightweight sources and detectors. These are based on interferometers that count the spacing between the resulting interference fringes [8–10], whereas some others use the space between the diffraction orders generated by a diffractive element which was utilized by Zemax software.

In addition, Zemax will manufacture normal analysis diagrams like ray-fan plots, spot diagrams, additionally as optical power plots. The advantages of the MZI provide flexibility in fringe localization that is not accessible with

*Corresponding author, E-mail: nhameed35@yahoo.com

different interferometers. Though an oblong quadrangle arrangement is usually utilized in MZI, quadrangle arrangements may also be shaped. The configuration of the MZI is versatile; thus it may be employed in many basic analysis topics like quantum physics [11], as well as studies on conditional determinateness, optical modulator [12] quantum computation, quantum trap, quantum logic, quantum cryptography, quantum Zeno impact, quantum implement experiment, quantum electronics and nucleon optical phenomenon [13, 14]. The MZI additionally permits to see the wavelength of the light beam, determination of the index of refraction of a transparent material and measures the index of refraction of air and completely different gases [15–17]. In this work, the theoretical and experimental results will be calculated by Zemax software and MZI, respectively. Then, these results will be compared. The diameters of fringes will be calculated by the optical system. This technique is considered easier and cheaper than other traditional techniques.

2. Methodology and Experimental Setup

In order to develop the characterization of the MZI, a setup is made as in Fig. 1. The diode laser represents the laser source of wavelength equals 0.65 μm and its power 5 mW. It is followed by the other elements that are fastened on the base plate, mirror (M1) was adjusted for alignment, mirror (M2) whose tilt is adjustable and might be translated with a screw. In addition, ray splitters (RS1 and RS2) were controlled by adjustable mounts. Mirror M2 is adapted with a micrometer spiral for the absolute adaptation of the mirror via a lever, in addition to two detectors A and B [18].

First of all, we need to know about the Fresnel equations which describe the phase shift and polarization of diffracted light when incident upon a medium of different refractive index in the case of MZI [19]. The incident angle is 45° and the Fresnel equations showed that a phase shift of π occurs when the incident light is reflected.

The initial medium has a lower refractive index than the medium which the light effect reflected this phase shift of

π. It used an interferometer to detect constructive and destructive interferences.

$$r_s = \frac{n_1 \cos \theta_i - n_2 \cos \theta_t}{n_1 \cos \theta_i + n_2 \cos \theta_t} \tag{1}$$

$$t_s = \frac{2n_1 \cos \theta_i}{n_1 \cos \theta_i + n_2 \cos \theta_t} \tag{2}$$

n1: Coefficient refraction of the first material, and

n2: Coefficient refraction of the second material

θi = Angle of incidence, and θt = Angle of refraction

Generally, the angle in MZI is 45°; when θi = 45° and n2 > n1

$$\theta_t = \sin^{-1} \left(\frac{n_1}{n_2} \sin 45^\circ \right) < 45^\circ$$

$$\therefore r_s < 0 \Rightarrow \text{phase shift } 0f(\pi).$$

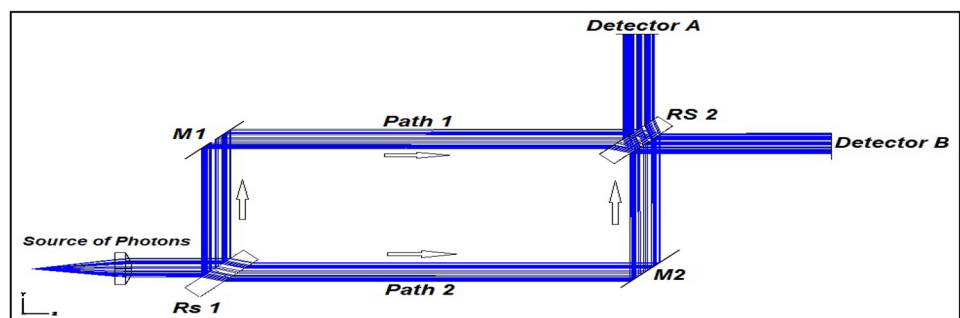
2.1. Empirical Setup

The question of how MZI works comes out of reading through A-level analysis and essays. The essential measuring system is illustrated as in Fig. 1 and it is explained that interference between the two paths ensures that the photon invariably strikes detectors A and B. First of all, the part of the photon on following every one of the two paths, path L1 and path L2, is considered. At the start, we tend to assume that there is no phase shift in reflection or transmission in the optical path length.

Before the first splitter on the transmission, no part shift is non-inheritable and on the reflection, a phase shift of π (180°) is obtained. Before ordinal splitter in path L1, there is a square that measures two reflections as a complete phase shift of two π. In path L2, there is a transmission and a reflection that complete phase shift of π. For detector A, path L1 can build a new transmission and therefore path L2 can endure a new reflection. Thus, the total phase shift from path L1 and path L2 is a pair of π.

For detector B, path L1 can endure a new reflection and therefore path L2 can build a new transmission. Hence, total phase shift from path L1 equals three π, and total

Fig. 1 Diagram of a simple MZI without the thickness of the ray splitters



phase shift from path L2 equals π [20]. In addition, the drawback of the MZI is that it does not work [21].

The devil during this case is within the detail of the phase shifts on reflection, thus the study does not provide straightforward answers.

2.2. Zemax Software Setup

The Zemax screen shows a tape of the tools at the top that includes the file, editor and system as shown in Fig. 2 of the experimental procedure of Zemax. Details of the Zemax parameters for the MZI are illustrated in Table 1.

3. Results and Discussion

MZI was used as the associated measuring device to measure the wavelength. The light constructively and destructively interfered once the position of the mirror (M2) was modified by micrometer as in Fig. 3. The pattern returned to a uniform position when the mirror was moved 1/2 wavelength for every time. The amounts of cycles were counted. Interference fringes were marked, so cycles were also counted more easily [22].

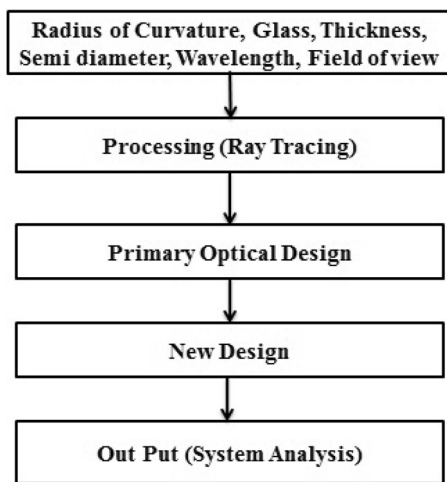


Fig. 2 Block diagram of design process

Table 1 Zemax parameters for the MZI

MZI	Value
Wavelength	0.65 μm
Wavenumber	1
Working $F/\#$	10,000
Power	0.005 W
Material	BK7

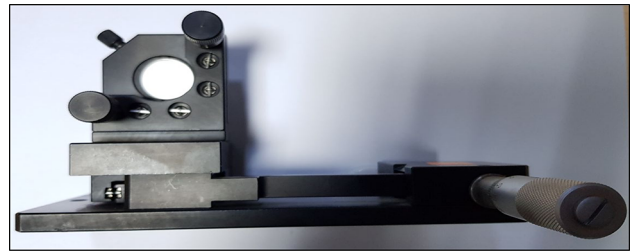


Fig. 3 The screws on the back of the mirror M2 used to vary the path difference between the two beams

The fringes could complete one cycle and a replacement fringe could be seen on the screen when the micrometer mirror was moved by 1/2 wavelength as in Fig. 3. The fringe contour pattern that is illustrated in Fig. 4a had been shifted in phase by $\pi/2$ with reference to that of Fig. 4b. Thus, investigation on the amount of twenty cycles can result from $d = 6.5 \mu\text{m}$. The wavelength can be calculated by applying the following formula (3).

$$\lambda = \frac{2d}{N} \tag{3}$$

d = the distance between two fringes. N = the number of fringes

$$\lambda = \frac{2 * (6.5)}{20} \mu\text{m} = 0.65 \mu\text{m}.$$

The temperature is not affected; here, the effect of it is appearance when the experiment was done in the chamber which contains one or mix of gases.

On the other hand, the Zemax simulation design is illustrated in Fig. 1. Also, Fig. 4 is the detector (a, b) laser output optical power. It can be seen that the fringe of detector A; phase shifted fringe of the detector B. We can see the similarities between the laser powers and the simulation as well as the experimental results. Figure 4 shows the resulting splitters between crossed polarizers when seen with a recognized laser source.

The dark rings relate to the regions where the spiraling optics axis is lined up with the polarizer or analyzer axis. Accordingly, the director angle changes by 45° between every dim ring. We define the grating pitch, to correspond to the director angle changing distance between splitters. Some point defects are observed in Fig. 5a, which may come from the dust in the spin coating process or particles not being totally filtered from the mirror or splitters (distance).

Line pairing is sometimes observed, depending on the exact method of focusing the fingers image by Zemax software. Also, Zemax in different radius are shown in Fig. 4.

The fringe of the detector simulations by Zemax and experimental setup of the proposal is shown in Figs. 4 and

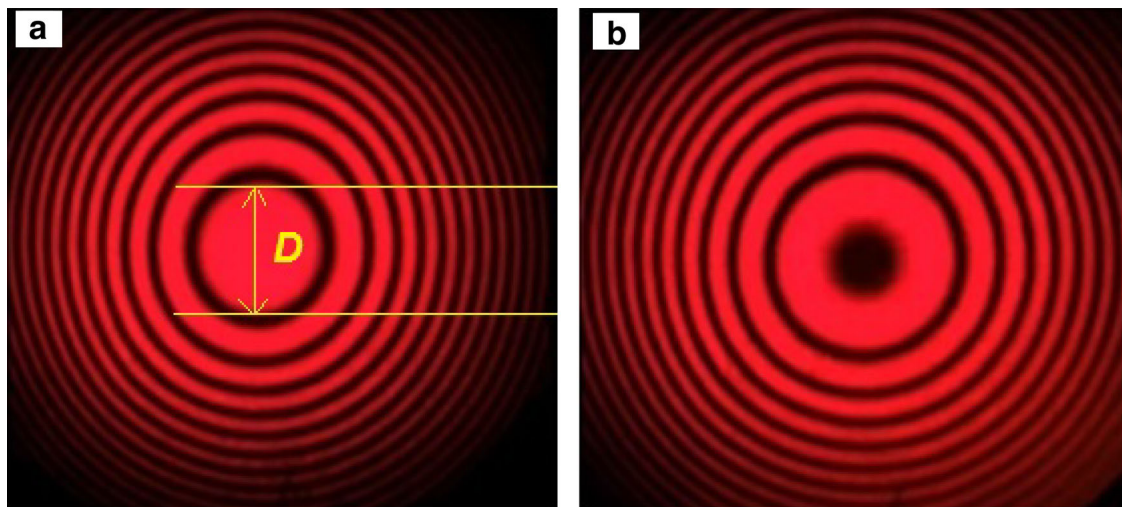


Fig. 4 Fringes on the screen **a** fringe contour pattern, **b** phase shifted fringe pattern

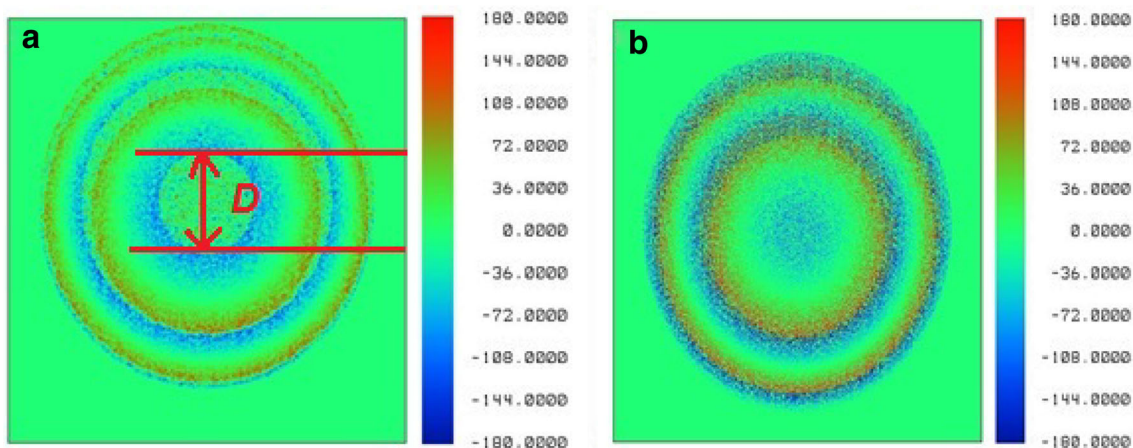


Fig. 5 Zemax simulation **a** fringe of the detector A, **b** phase shifted fringe of the detector B

5, during which thanks to the relation between the size of the chosen pinhole and its distance to the visual image screen; the resulting airy pattern meets the characteristics corresponding to a diffraction that shows the ring mount wherever a piece of vellum paper has been used as a visualization screen. It will be shown that the size of the inner diameter not clear of this mount was used to calibrate the system; therefore, the size of the airy disk in pixels should be remodeled in real spatial units (cm).

The comparison of simulations and experimental results is further discussed as follows. The manufacturer’s data for the Zemax simulation comprise the experimental output

fringe. According to Table 2, the comparison of simulations and experiments of the laser is in agreement [23].

The shining ring in the centermost is accepted as the airy disk which contains 84% of the high energy. We can calculate the angular diameter by the formula (4)

$$B_{\text{ang}} = \frac{2.44 * \lambda}{D} \tag{4}$$

In the formula, B is the wavelength of the airy disk angular diameter; D is the diameter of the optical system.

$$B_{\text{Diff}} = B_{\text{ang}}f = \frac{2.44\lambda * f}{D} = 2.44 * \lambda(F/\#)$$

Table 2 Summary of the results of the simulations and experiments

Wavelength (λ)	Airy diameter D (experiment)	Angular diameter B (experiment)	Airy diameter D (simulation)	Angular diameter B (simulation)
0.65 μm	1.16 cm	1.36 cm	1.11 cm	1.42 cm

It is worth noting that Table 2 shows the agreement for this simulation and experiments as well as the characteristics and materials obtained from the diameter D measurements, thus many sources of error were investigated.

In order to validate the proposal, the resulting average of the two airy diameter D and B experiments was compared with the two airy diameter D and B simulation provided by the manufacturer corresponding to the laser sources by calculating the percentage error:

$$\begin{aligned} \%_{\text{error}_D} &= \left| \frac{\text{Airy diameter } D \text{ (experiment)} - \text{Airy diameter } D \text{ (simulation)}}{\text{Airy diameter } D \text{ (simulation)}} \right| \\ \%_{\text{error}_B} &= \left| \frac{\text{Angular diameter } B \text{ (experiment)} - \text{Angular diameter } B \text{ (simulation)}}{\text{Angular diameter } B \text{ (simulation)}} \right| \\ \%_{\text{error}_D} &= \left| \frac{1.16 - 1.11}{1.11} \right| = 0.05\% \\ \%_{\text{error}_B} &= \left| \frac{1.36 - 1.42}{1.42} \right| = 0.04\% \end{aligned}$$

According to the calculation of percentage error, it is possible to conclude that the proposal presents a simple and feasible methodology to estimate the two airy diameters D and B experiments.

Through the course of this article, we have introduced the basics of work systems and sources modeled the base system; a Michelson interferometer demonstrated the coherence gate effect which enables depth scanning. Our system is now ready to be used as an experimental model by Zemax program. We can add custom or commercial lenses to the sample arm to test the impacts on spot size or the focal position within the sample, or a spectrometer could be added to the output leg to model broadband Fourier domain measurements. Alternatively, more complex samples can be simulated, from simply adding multiple reflective surfaces to simulate multiple re-emitting points in the sample, to importing tissue models such as Zemax's human eye.

4. Conclusions

In this paper, we have highlighted a different, conferred and cheap technique to estimate the wavelength of an optical device supplied by experiments. MZI and simulation by Zemax were used in this study. These results were in agreement theoretically and experimentally. It was found that the fringes pattern analysis has a serious impact on interferometry.

In this different technical research, it is not required to use other optical meters or devices that represent potential search work in optical or physical laboratories, besides the increase in expenses. And additionally through the

utilization of the Zemax program, we will powerfully believe that this proposal provides an awfully good approximation and is utterly appropriate to be applied for didactical, academic or demonstrative purposes in topics that involve optical phenomena and ideas similar to diffraction and the wavelength for collegian or graduate students within the field of physics or where these concepts are connected.

References

- [1] L. Zehnder, Ein neuer interferenzrefraktor, Springer, Berlin, (1891).
- [2] L. Zehnder, Instrum. Z., **11** (1891) 275.
- [3] Z. Ludwig Mach, Instrumentenkunde., **12** (1892) 89.
- [4] J.M. Simon, S.A. Comastri and R.M. Echarri, The Mach-Zehnder interferometer: examination of a volume by non-classical localization plane shifting, J. Opt. A Pure Appl. Opt., **3** (2001) 242.
- [5] J. Simon, M. Simon, R. Echarri and M. Garea, Fringe localization in interferometers illuminated by a succession of incoherent line sources, J. Mod. Opt., **45** (1998) 2245–2254.
- [6] F. Boudaoud and M. Lemerini, Using a Mach-Zehnder interferometer to deduce nitrogen density mapping, Chin. Phys. B, **24** (2015) 075205.
- [7] Y. Zhou, T. Shen, B. Sun and Y. Feng, Research and development of testing aspheric surfaces using two-wavelength interferometer methods, Information science and electronic engineering: proceedings of the 3rd international conference of electronic engineering and information science (ICEEIS 2016), January 4–5, 2016, CRC Press, Harbin (2016) p. 297.
- [8] P. Fox, R. Scholten, M. Walkiewicz and R.E. Drullinger, A reliable, compact, and low-cost Michelson wavemeter for laser wavelength measurement, Am. J. Phys., **67** (1999) 624–630.
- [9] T. Catunda, J. Sartori and L. Nunes, Plane wave interference: a didactic experiment to measure the wavelength of light, Am. J. Phys., **66** (1998) 548–549.
- [10] A. Kahane, M. O'Sullivan, N. Sanford and B. Stoicheff, Vernier fringe-counting device for laser wavelength measurements, Rev. Sci. Instrum., **54** (1983) 1138–1142.
- [11] A. Roy and S. Ghosh, Evolution of photon beams through a nested Mach-Zehnder interferometer using classical states of light. arXiv preprint [arXiv:1701.03074](https://arxiv.org/abs/1701.03074) [quant-ph] (2017).
- [12] A. Hanim, H. Hazura, S. Idris, A.M. Zain, F. Salehuddin and A.H. Afifah-Maheran, Performance of different Mach-Zehnder interferometer (MZI) structures for optical modulator, J. Telecommun. Electron. Comput. Eng. (JTEC), **9** (2017) 25–29.
- [13] K. Bartkiewicz, A. Černoch, D. Javůrek, K. Lemr, J. Soubusta and J. Svozilík, One-state vector formalism for the evolution of a quantum state through nested Mach-Zehnder interferometers, Phys. Rev. A, **91** (2015) 012103.
- [14] N. Garg, K. Soni, A. Kumar and T Saxena, Applications of laser interferometry in providing traceable vibration measurements in India, MAPAN-J. Metrol. Soc India, **30** (2015) 91–104.
- [15] M.G. Paris, Entanglement and visibility at the output of a Mach-Zehnder interferometer, Phys. Rev. A, **59** (1999) 1615.
- [16] G. Haack, H. Förster and M. Büttiker, Parity detection and entanglement with a Mach-Zehnder interferometer, Phys. Rev. B, **82** (2010) 155303.
- [17] M. Bahrawi and N. Farid, Application of a commercially available displacement measuring interferometer to line scale

- measurement and uncertainty of measurement, MAPAN-J. Metrol. Soc India, **25** (2010) 259–264.
- [18] E.I. Pacheco-Chacon, E. Gallegos-Arellano, J.M. Sierra-Hernandez, R. Rojas-Laguna, J.M. Estudillo-Ayala, E. Hernandez, D. Jauregui-Vazquez and J.C. Hernandez-Garcia, Torsion sensing setup based on a Mach–Zehnder interferometer with photonics crystal fiber, Photonic Instrumentation Engineering IV: International Society for Optics and Photonics (2017) p. 101100V.
- [19] S. Srisuwan, C. Sirisathitkul and S. Danworaphong, Validation of photometric ellipsometry for refractive index and thickness measurements, MAPAN-J. Metrol. Soc India, **30** (2015) 31–36.
- [20] L. Fu, F. Hashmi, Z. Jun-Xiang and Z. Shi-Yao, An ideal experiment to determine the ‘past of a particle’ in the nested Mach–Zehnder interferometer, Chin. Phys. Lett., **32** (2015) 050303.
- [21] R.B. Griffiths, Particle path through a nested Mach–Zehnder interferometer, Phys. Rev. A, **94** (2016) 032115.
- [22] G. Reid, Automatic fringe pattern analysis: a review, Opt. Lasers Eng., **7** (1986) 37–68.
- [23] U. Rivera-Ortega and B. Pico-Gonzalez, Wavelength estimation by using the Airy disk from a diffraction pattern with didactic purposes, Phys. Educ., **51** (2015) 015012.

Publisher’s Note Springer Nature remains neutral with regard to jurisdictional claims in published maps and institutional affiliations.